

# Another brick in understanding chemical and kinematical properties of BSSs: NGC 6752 <sup>1</sup>

L. Lovisi<sup>1</sup>, A. Mucciarelli<sup>1</sup>, E. Dalessandro<sup>1</sup>, F.R. Ferraro<sup>1</sup>, B. Lanzoni<sup>1</sup>

<sup>1</sup> *Dipartimento di Fisica & Astronomia, Università degli Studi di Bologna, viale Berti Pichat 6/2, I-40127 Bologna, Italy*

## ABSTRACT

We used high-resolution spectra acquired with the multifiber facility FLAMES at the Very Large Telescope of the European Southern Observatory to investigate the chemical and kinematical properties of a sample of 22 Blue Straggler Stars (BSSs) and 26 red giant branch stars in the nearby globular cluster NGC 6752. We measured radial and rotational velocities and Fe, O and C abundances. According to radial velocities, metallicity and proper motions we identified 18 BSSs as likely cluster members. We found that all the BSSs rotate slowly (less than  $40 \text{ km s}^{-1}$ ), similar to the findings in 47 Tucanae, NGC 6397 and M30. The Fe abundance analysis reveals the presence of 3 BSSs affected by radiative levitation (showing  $[\text{Fe}/\text{H}]$  significantly higher than that measured in “normal” cluster stars), confirming that element transport mechanisms occur in the photosphere of BSSs hotter than  $\simeq 8000 \text{ K}$ . Finally, BSS C and O abundances are consistent with those measured in dwarf stars. No C and O depletion ascribable to mass transfer processes has been found on the atmospheres of the studied BSSs (at odds with previous results for 47 Tucanae and M30), suggesting the collisional origin for BSSs in NGC 6752 or that the CO-depletion is a transient phenomenon.

*Subject headings:* blue stragglers; globular clusters: individual (NGC 6752); stars: abundances; stars: evolution; techniques: spectroscopic;

## 1. Introduction

Galactic globular clusters (GCs) are dynamically active stellar systems where interactions and collisions, especially involving binaries, are quite frequent (Hut et al. 1992;

---

<sup>1</sup>Based on FLAMES observations collected at the European Southern Observatory, proposal numbers 081.D-0356 and 089.D-0298.

Meylan & Heggie 1997). These interactions likely generate exotic objects like X-ray binaries, millisecond pulsars and Blue Straggler stars (BSSs; see Paresce et al. 1992; Baily 1995; Bellazzini et al. 1995; Ferraro et al. 1995, 2009; Ransom et al. 2005; Pooley & Hut 2006). BSSs are the most abundant products of this activity. They are brighter and bluer than the main sequence (MS) turnoff (TO). They lie along an extension of the MS and they are known to be more massive than normal TO stars (Shara et al. 1997; Gilliland et al. 1998; De Marco et al. 2005). Because of their mass, BSSs are invaluable probes of GC internal dynamics. In particular, it has recently shown that their radial distribution is a powerful tool to measure the cluster dynamical age (Ferraro et al. 2012). Nevertheless, many basic questions about the formation mechanisms and the physical properties of these puzzling objects remain open. Two main scenarios have been proposed for their formation: they could form through mass transfer in a binary system that could lead to the complete coalescence of the two companions (MT-BSSs; McCrea 1964) or through stellar collisions (COL-BSSs; Hills & Day 1976). Hydrodynamic simulations suggest different chemical patterns for BSSs formed through the two different mechanisms. In particular, MT-BSSs are expected to show C and O depletion (Sarna & De Greve 1996) whereas no chemical anomalies are predicted for COL-BSSs (Lombardi et al. 1995). On the contrary, predictions about the BSS rotational velocity  $v_e \sin(i)$  are quite controversial. In fact, both MT- and COL-BSSs are expected to rotate fast (Benz & Hills 1987; Sarna & De Greve 1996), but accurate simulations are lacking for MT-BSSs and braking mechanisms may intervene both for MT- and COL-BSSs slowing down the initial BSS rotation, with timescales and efficiencies still unknown (Leonard & Livio 1995; Sills et al. 2005).

In addition to GCs, BSSs have been detected in a variety of low-density environments such as Galactic open clusters (Ahumada & Lapasset 1995), dwarf spheroidal galaxies in the Local Group (Momany et al. 2007), the Milky Way’s bulge (Clarkson et al. 2011) and halo (Preston & Sneden 2000; Sneden et al. 2003; Carney et al. 2005) and, recently, also ultra-faint galaxies (Santana et al. 2013). Despite less populous than GCs, these low-density systems contain a high percentage of BSSs. However, the low collisional rate in low-density environments implies a different origin for the BSSs in GCs and loose systems, where BSSs likely formed exclusively by MT.

In this framework, we started an observational campaign aimed at performing the first systematic study of the chemical and kinematical properties of BSSs in GCs and at studying their possible differences in MT- and COL-BSSs. Spectroscopic results by Ferraro et al. (2006) have observationally revealed the presence of a subpopulation of CO-depleted BSSs in 47 Tucanae and similarly Lovisi et al. (2013) identified 4 BSSs with O upper limits incompatible with the cluster O abundance in M30. In both cases, the amount of the observed C and O depletion is incompatible with that expected for second generation stars (predicted

to be C and O poor) and cannot be interpreted in terms of self-enrichment processes. On the contrary, Lovisi et al. (2010) found no evidence of CO-depleted BSSs in M4, whereas no interpretation in terms of formation mechanism was possible for the BSSs studied by Lovisi et al. (2012) in NGC 6397, due to the occurrence of a diffusion process, called radiative levitation, that alters chemical abundances on the surfaces of stars with shallow or no-convective envelopes. Ferraro et al. (2006) identified only one fast rotating ( $v_e \sin(i) > 50 \text{ km s}^{-1}$ ) BSS in 47 Tucanae, corresponding to  $\sim 2\%$  of the studied population. A similar fraction of fast rotating BSSs has been also found by Lovisi et al. (2012) and Lovisi et al. (2013) (respectively  $\sim 5\%$  and  $\sim 6\%$ ). Surprisingly, Lovisi et al. (2010) found that 40% of the studied BSS population in M4 rotate faster than  $50 \text{ km s}^{-1}$ .

In this work, we discuss the properties of a BSS sample in NGC 6752. The paper is structured as follows: the observations are described in Sect. 2. The determination of stellar radial velocities and cluster membership are discussed in Sect. 3. The estimate of atmospheric parameters is described in Sect. 4. The measured rotational velocities are presented in Sect. 5. Sect. 6 describes methods and results of the chemical abundance analysis for our sample. Finally our conclusions are drawn in Sect. 7.

## 2. Observations

This work is based on the analysis of spectra of individual stars in NGC 6752, obtained with the multi-object facility FLAMES (Pasquini et al. 2002) mounted at the Unit Telescope 2 at the Very Large Telescope of the European Southern Observatory. Observations were performed during two different runs (081.D-0356 and 089.D-0298, hereafter P81 and P89, respectively) with the UVES+GIRAFFE combined mode, during the nights 2008 August 13-16 and 2012 July 4. Spectra have been acquired for 22 BSSs and 26 red giant branch (RGB) stars, most of them being observed in both P81 and P89. Four different setups have been used for the spectroscopic observations: HR5A (with spectral coverage 4340-4587 Å and spectral resolution  $R=18470$ ), HR15N (6470-6790 Å,  $R=17000$ ), HR18 (7468-7889 Å,  $R=18400$ ) and HR22A (8816-9565 Å,  $R=11642$ ), suitable to sample some metallic lines, the  $H\alpha$  line, the O I triplet at  $\simeq 7774 \text{ Å}$  and two C I lines at 9078.3 and 9111.8 Å, respectively. Multiple exposures for each target have been secured according to the efficiency of the different setups, in particular 5 exposures with HR5A, 2 with HR15N and 4 with HR18 and HR22A have been obtained. The total exposure times amount to 3.75 hours for the HR5A, 1.5 hours for the HR15N and 3 hours for the HR18 and HR22A. The spectroscopic target selection has been performed from a photometric catalog obtained by combining ACS@HST data in V and I bands for the central regions and WFI@ESO observations in B and R

bands for the external regions. Fig. 1 shows the CMDs for the ACS and WFI datasets, with the position of all the analyzed targets. The spectra pre-reduction has been performed by using the latest version of the GIRAFFE ESO pipeline (*gasgano* version 2.4.3<sup>2</sup>), that includes bias subtraction, flat-field correction, wavelength calibration and one-dimensional spectra extraction. For each exposure we subtracted the corresponding master sky spectrum, obtained by averaging several spectra of sky regions. By combining the sky-subtracted exposures, we obtained median spectra with signal-to-noise ratios  $S/N \simeq 30 - 120$  for the selected BSSs, and  $S/N \simeq 50 - 150$  for the RGB stars.

### 3. Radial velocities

#### 3.1. Cluster membership

In order to assess cluster membership for each target, radial velocities (RVs) have been measured with the IRAF task *fxcor* following the technique described by Tonry & Davis (1979). Synthetic spectra calculated with the atmospheric parameters of the analyzed targets (see Sect. 4) and convolved with a Gaussian profile to reproduce the spectral resolution of the corresponding GIRAFFE setup, have been used as templates for the cross-correlation (see Sect. 5 for details about the computation of the synthetic spectra). Finally, the heliocentric correction has been applied to all the RVs. Tables 1 and 2 show the mean heliocentric RVs obtained as the average of values in P81 and P89.

The mean radial velocity of the RGB stars is  $RV = -26.7 \pm 0.8 \text{ km s}^{-1}$  ( $\sigma = 4.0 \text{ km s}^{-1}$ ) which is fully in agreement with previous results by Harris (1996, 2010 edition) and Carretta et al. (2009). The derived RV distribution for the RGB stars is shown in Fig. 2 (main panel, empty histogram). The mean RV of the RGB stars has been assumed as the systemic velocity of NGC 6752 and used to infer cluster membership for BSSs: stars having RVs within  $3\sigma$  from the systemic velocity value have been considered as members of the cluster. The mean radial velocity of the 22 observed BSSs is  $RV = -16.9 \pm 0.8 \text{ km s}^{-1}$  ( $\sigma = 40.5 \text{ km s}^{-1}$ ) but the  $3\sigma$ -rejection based on the results of the RGB stars leads to the identification of 4 BSSs (with  $RV = -92.8, -14.1, 97.2, 110.7 \text{ km s}^{-1}$ ) as possible non-members. However, particular discussion deserves BSS13. This star has  $RV = -14.1 \text{ km s}^{-1}$  so that it is within  $3.5\sigma$  from the mean RV and it is located very close ( $23.8''$ ) to the cluster centre. Moreover, its iron content is fully in agreement with the mean cluster metallicity (see Sect. 6). By using Besançon Galactic model by Robin et al. (2003)<sup>3</sup>, we derived the metallicity distribution of field stars

---

<sup>2</sup><http://www.eso.org/sci/software/pipelines/>

<sup>3</sup><http://model.obs-besancon.fr/>

in the direction of NGC 6752, within the same magnitude and colour intervals shared by our BSS sample. We computed that the probability to observe a field star with an iron content similar to that of BSS13 ( $[\text{Fe}/\text{H}] = -1.43$ ) is 1.4%. For this reason, we decided to consider BSS13 as cluster member and to include it in our sample.

As shown in the inset of Fig. 2 the systemic velocity of NGC 6752 is very similar to the peak of the RV distribution of field stars in the direction of the cluster (Robin et al. 2003), so that the probability of field contamination among the BSSs is very high and the measure of radial velocities cannot totally guarantee the cluster membership. Therefore, in order to further constrain the membership of BSSs in our sample, we used proper motions: we performed a cross-correlation between our BSS sample and the catalog of Zloczewski et al. (2012) by using the software CataXcorr (P.Montegriffo, private communication). We found 9 BSSs in common. According to their proper motions, one BSS in our sample (with  $\text{RV} = -22.7 \text{ km s}^{-1}$ , totally in agreement with the systemic velocity) certainly belongs to the field, one (namely BSS5) is a possible cluster member, whereas the remaining 7 stars (namely BSS1, BSS10, BSS11, BSS14, BSS15, BSS16 and BSS17) are likely members. After removing non-member BSSs (large black dots in Fig. 1) from our sample, we are left with 18 BSSs that are likely cluster members (open circles in Fig. 1). The RV distribution for these stars is shown in Fig. 2 (grey shaded histogram). The mean value is  $\text{RV} = -25.5 \pm 0.9 \text{ km s}^{-1}$  ( $\sigma = 5.9 \text{ km s}^{-1}$ ), in good agreement with the mean value inferred from the RGB stars.

In our sample we found 8 variable stars. In particular, BSS6, BSS10, BSS11 and BSS17 correspond to V21, V17, V12 and V7 studied by Kaluzny & Thompson (2009). In particular, BSS11 and BSS17 are classified as SX-Phoenicis whereas BSS6 is likely a  $\gamma$  Dor type pulsator and BSS10 has been classified as a possible binary composed of a hot extreme-Horizontal Branch star (EHB) and a red companion on the basis of its location in the CMD.

We have measured RV variation of  $\sim 13 \text{ km s}^{-1}$  and  $\sim 5 \text{ km s}^{-1}$  between P81 and P89 for BSS11 and BSS17, both classified as SX-Phoenicis. Moreover, for BSS11 we observe differences in the RV also between individual HR5A exposures (up to  $\sim 25 \text{ km s}^{-1}$ ). Given the duration of our exposures (45 minutes each), the variation of RV is in agreement with the period found by Kaluzny & Thompson (2009) for those SX-Phoenicis ( $\sim 85$  and  $\sim 59$  minutes). However, we stress that the time sampling of our data set is not suitable to perform an accurate investigation of the radial velocity variability that can reveal possible binary stars. This does not rule out the possibility that some of the BSSs in our sample belong to binary systems.

### 3.2. The nature of BSS10

A further clarification should be done also for BSS10. Based on its position in the CMD, Kaluzny & Thompson (2009) suggested that this star could be an unresolved binary system formed by an EHB star and a red companion. As suggested by Ferraro et al. (1997, 2004), the optimal way to observe hot stars like BSSs and Horizontal Branch stars is at ultraviolet (UV) wavelengths. In fact, in this plane RGB stars (the brightest objects in the optical CMD) are faint and the identification of hot stars is very easy. Therefore, in order to investigate the possibility that BSS10 could be an unresolved binary system, we identified it in the UV WFPC2 catalog used by Sabbi et al. (2004). According to its position in the UV plane (see Fig. 3) we can conclude that BSS10 is too faint to be an EHB, but it is instead one of the brightest BSSs in NGC 6752. We suggest that the variability observed in the light curve by Kaluzny & Thompson (2009) might be due to a BSS in a binary system with a low-mass MS companion.

## 4. Atmospheric parameters

Effective temperature ( $T_{eff}$ ) and surface gravity ( $\log g$ ) for all the observed targets have been derived comparing their position in the CMD with theoretical isochrones (with different ages) from the Padova database <sup>4</sup> (Bressan et al. 2012). Given the stellar position in the CMD, each observed target has been orthogonally projected on the closest theoretical model, and  $T_{eff}$  and  $\log g$  have been derived for each star. For the RGB stars, an isochrone of 12 Gyr,  $Z=0.0005$  and  $\alpha$ -enhanced chemical mixture has been superimposed on the CMD of NGC 6752, assuming a distance modulus  $(M-m)_0 = 13.18$  and  $E(B-V)=0.04$  (Ferraro et al. 1999). For BSSs, isochrones with different ages (2-8 Gyrs, and assuming the same chemical composition, distance modulus and reddening values) have been used to sample the BSS region.

The atmospheric parameters for the BSS and RGB samples are listed in Tables 1 and 2, respectively. Conservative errors in temperatures and gravities have been considered: 100 K and 0.2 dex both for BSSs and RGB stars. Concerning microturbulent velocity, the small number of metallic lines prevents us to derive spectroscopically this parameter. For this reason, we assumed  $2.0 \text{ km s}^{-1}$  and  $1.5 \text{ km s}^{-1}$  for BSS and RGB stars, respectively. We finally adopted a conservative error of  $0.5 \text{ km s}^{-1}$  for all the targets.

---

<sup>4</sup><http://stev.oapd.inaf.it/cgi-bin/cmd>.

## 5. Rotational velocities

Rotational velocities have been derived for all the targets through a  $\chi^2$  minimization between the observed spectrum and a grid of synthetic spectra, computed for all stars by adopting the estimated atmospheric parameters and different rotational values. All the synthetic spectra have been computed by using the Kurucz’s code SYNTHE (Kurucz 1993; Sbordone et al. 2004), including the atomic data for all the lines from the most updated version of the Kurucz line list by F.Castelli <sup>5</sup>. Model atmospheres for the synthetic spectra have been calculated with ATLAS9 code (Kurucz 1993; Sbordone et al. 2004) under the assumptions of Local Thermodynamic Equilibrium (LTE) and plane-parallel geometry and adopting the new opacity distribution functions by Castelli & Kurucz (2003), without the inclusion of the approximate overshooting (Castelli et al. 1997). The most prominent features in the stellar spectra have been used to infer stellar rotations. In particular, for the RGB stars  $v_e \sin(i)$  values have been inferred from the Ba II at 4554.03 Å whereas for BSSs from the Mg II line at 4481 Å and the O I line at 7771.95 Å. Typical uncertainties in the  $v_e \sin(i)$  measurement are of the order of few  $\text{km s}^{-1}$ .

The rotational velocity distribution thus obtained for BSSs is shown in Fig. 4 (upper panel) and it is compared with that of RGB stars (lower panel). Almost all RGB stars have  $v_e \sin(i) = 0 \text{ km s}^{-1}$ , the largest value not exceeding  $6 \text{ km s}^{-1}$  (but with uncertainties that make them compatible with  $v_e \sin(i) \sim 0 - 1 \text{ km s}^{-1}$ ). These results are in agreement with those usually observed for this kind of stars (see e.g. Carney et al. 2008; Cortés et al. 2009; Mucciarelli et al. 2011; Lovisi et al. 2013). On the contrary, the rotational velocity distribution of BSSs is much wider: some BSSs show the same average  $v_e \sin(i)$  of RGB stars but others have rotational velocities several times larger, up to the highest value of  $\sim 38 \text{ km s}^{-1}$ .

Finally, Fig. 5 (upper panel) shows the rotational velocity as a function of temperature for all the targets: for each temperature value high spread in  $v_e \sin(i)$  is observed.

## 6. Chemical abundances

Iron abundances have been measured for all BSSs and compared with those derived from the RGB stars. Oxygen abundances for BSSs have been derived from the O I triplet at  $\sim 7774$  Å and carbon abundances from two C I lines at 9078.3 and 9111.8 Å. No determination of O and C abundances is possible for RGB stars of our sample, since their temperatures are too

---

<sup>5</sup><http://wwwuser.oat.ts.astro.it/castelli/linelists.html>

low to detect O and C lines in the studied spectral ranges. Abundances for all the targets have been estimated with the code GALA (Mucciarelli et al. 2013a) by using the measured equivalent widths (EWs) of the absorption lines. EWs for RGB stars have been measured with DAOSPEC (Stetson & Pancino 2008) whereas for BSSs we used our own FORTRAN procedure (Mucciarelli et al. 2011) that has the advantage to perform a Gaussian fit on a spectral window selected interactively, in order to optimize the line fitting procedure also for moderate rotating stars. The used reference solar abundances are from Grevesse & Sauval (1998) for Fe and C and from Caffau et al. (2011) for O.

Possible deviations from the LTE assumption have been taken into account. Non-LTE corrections for O abundances have been taken from Gratton et al. (1999) and Takeda (1997) for BSSs colder and hotter than 8000 K respectively, and corrections from Tomkin et al. (1992) have been used for C abundances. Conversely, no grid of non-LTE corrections are available in the literature for iron lines for the range of parameters typical of our BSSs. Based on the fact that non-LTE corrections for ionized elements in warm (A and F type) stars are negligible with respect to those for neutral elements, we obtained Fe abundances for the BSSs by using Fe II lines, whereas Fe I lines have been used for the RGB stars (for which the LTE approximation is still valid). Fe, C and O abundances for BSSs and RGB stars are listed in Table 1 and 2, respectively.

**Iron** – For the RGB stars we find an average iron abundance of  $[\text{Fe}/\text{H}] = -1.53 \pm 0.01$  ( $\sigma = 0.07$ ) dex in very good agreement with results by Carretta et al. (2009) and Yong et al. (2013). The mean iron abundance for BSSs is  $[\text{Fe}/\text{H}] = -1.41 \pm 0.01$  ( $\sigma = 0.29$ ), that is 0.1 dex higher and more scattered than that of the RGB stars. Fig. 5 (lower panel) shows the comparison between the iron distributions of RGB stars (grey triangles) and BSSs (open circles and squares) as a function of temperatures: most of the BSSs show Fe values in agreement with the mean iron abundance for the RGB stars (grey dashed horizontal line), nevertheless the 3 hottest BSSs ( $T_{\text{eff}} > 8000$  K, open squares in Fig. 5) show higher Fe abundances. The mean Fe abundance for BSSs colder than 8000 K is  $[\text{Fe}/\text{H}] = -1.52 \pm 0.02$  ( $\sigma = 0.10$ ), nicely matching the value found for the RGB stars.

**Carbon and oxygen** –  $[\text{C}/\text{Fe}]$  and  $[\text{O}/\text{Fe}]$  ratios for BSSs not affected by radiative levitation are shown in Fig. 6. In order to consistently compare C and O abundances for BSSs with those of a parent population, we used results by Carretta et al. (2005) obtained for dwarf stars (grey region in Fig. 6): BSS abundances well overlap the mean locus defined by the dwarf stars. Carbon and oxygen content for all BSSs colder than 8000 K is  $[\text{C}/\text{Fe}] = -0.12 \pm 0.08$  ( $\sigma = 0.29$ ) and  $[\text{O}/\text{Fe}] = +0.12 \pm 0.07$  ( $\sigma = 0.24$ ).

## 7. Discussion

### 7.1. Rotational velocities

Rotational velocities have been derived for the BSSs and compared with values obtained for the RGB stars. The BSS distribution is wider than the RGB one but no fast rotating ( $v_e \sin(i) > 50 \text{ km s}^{-1}$ ) BSSs have been found. In fact, apart from M4 (which is the most extreme case, Lovisi et al. 2010) where  $\sim 40\%$  of BSSs have been found rotating faster than  $50 \text{ km s}^{-1}$ , the other clusters studied so far (47 Tucanae Ferraro et al. 2006, NGC 6397 Lovisi et al. 2012, and M30 Lovisi et al. 2013) show a small fraction of fast rotating BSSs ( $\sim 2\%$ ,  $\sim 5\%$ ,  $\sim 6\%$  respectively, that are also WUma or SX-Phoenicis stars). Assuming these low percentages, we should have found at most one fast rotating BSS. It is interesting to note that all the investigated clusters showing a small fraction of fast rotating BSSs are high density clusters, possibly dynamically evolved. In fact, all of them belong to the oldest groups of Family II or Family III in the dynamical classification proposed by Ferraro et al. (2012). Indeed, NGC 6397 and M30 are post-core collapsed clusters and NGC 6752 is suspected to be in the post-core collapse bounce (Ferraro et al. 2003).

### 7.2. Chemical abundances

**Iron** – As shown in Sect. 3.1, Fe abundances for the observed BSSs help us to discriminate possible field stars. The  $[\text{Fe}/\text{H}]$  ratios for almost all BSSs agree very well with that derived for RGB stars and with previous results by other authors, excluding that these BSSs belong to the field. The only exceptions are BSS1 ( $[\text{Fe}/\text{H}] = -1.22$ ), BSS2 ( $[\text{Fe}/\text{H}] = -0.96$ ) and BSS10 ( $[\text{Fe}/\text{H}] = -0.46$ ). Nevertheless, from Fig. 5 it is clear that these stars are also the hottest ones in our sample, with  $T_{eff} > 8000 \text{ K}$ . Lovisi et al. (2012) and Lovisi et al. (2013) observed the same behavior (the hottest BSSs were also the most metallic ones) in several BSSs of NGC 6397 and M30. These results have been interpreted in terms of the occurrence of radiative levitation in the shallow convective envelopes of BSSs. Radiative levitation is a diffusion process that occurs when radiative acceleration exceeds the gravitational one (Michaud et al. 1983): therefore, many chemical elements are pushed toward the stellar surface and the original chemical composition is altered (in particular, the iron-peak elements abundances are enhanced with respect to the original chemical composition). In this framework, we conclude that also BSS1, BSS2 and BSS10 in NGC 6752 suffer from radiative levitation. Fig. 7 shows the  $[\text{Fe}/\text{H}]$  ratio for all the BSS samples in NGC 6397, M30 and NGC 6752 as a function of temperature. In order to compare in a meaningful way the iron abundances for BSSs in clusters with different metallicity, BSS  $[\text{Fe}/\text{H}]$  ratios have

been scaled to the mean cluster metallicities ( $[\text{Fe}/\text{H}] = -2.12$  for NGC 6397, Lovisi et al. 2012,  $[\text{Fe}/\text{H}] = -2.28$  for M30, Lovisi et al. 2013 and  $[\text{Fe}/\text{H}] = -1.53$  for NGC 6752, in this work. A clear trend with temperature exists and an abrupt increase in the  $[\text{Fe}/\text{H}]$  ratio is observed for BSSs hotter than 7800 K (dashed grey line). Independently from the cluster metallicity, the BSS iron abundance systematically increases with  $T_{\text{eff}}$  up to more than 2 dex.

**Carbon and Oxygen** – Carbon and oxygen surface abundances can be used as tracers of mass transfer processes where the donor star is peeled down to regions where the CNO-cycle occurred (Ferraro et al. 2006; Mucciarelli et al. 2013b). In particular C and O depletion are expected for MT-BSSs (Sarna & De Greve 1996) whereas no chemical anomaly should appear on the COL-BSSs surface (Lombardi et al. 1995). The first observational confirmation has been provided by Ferraro et al. (2006) that discovered 6 out of 42 CO-depleted BSSs in 47 Tucanae. Moreover, Lovisi et al. (2013) identified 4 BSSs with O upper limits incompatible with the cluster O abundance in the GC M30. These stars lie along the BSS red sequence that has been interpreted by Ferraro et al. (2009) as the one formed by MT-BSSs, at odds with the blue one formed by COL-BSSs. On the contrary, no evidence of CO-depletion has been found in M4 (Lovisi et al. 2010) whereas in the case of NGC 6397 the occurrence of radiative levitation on the surface of almost all the BSSs in the sample, prevents the interpretation of O abundances in terms of BSS formation mechanisms (Lovisi et al. 2012).

C and O abundances for the BSSs not affected by radiative levitation in NGC 6752 are in agreement with those derived for dwarf stars (Carretta et al. 2005). No CO-depleted BSSs have been identified in the studied sample. As suggested by Ferraro et al. (2006) the CO-depletion could be a transient phenomenon and "evolved" MT-BSSs might have restored their original chemical abundances. According to the percentage of CO-depleted BSSs in 47 Tucanae (14%), we could have expected 1-2 CO-depleted stars in NGC 6752. The lack of chemical anomalies in the studied sample might suggest that all the (investigated) BSSs in NGC 6752 may derive from stellar collisions, for which no chemical anomalies are expected. This features is again in agreement with the particular dynamical state proposed for NGC 6752 by Ferraro et al. (2003).

This research is part of the project COSMIC-LAB ([www.cosmic-lab.eu](http://www.cosmic-lab.eu)) funded by the European Research Council (under contract ERC-2010-AdG-267675). We thank the anonymous referee for his/her valuable suggestions.

## REFERENCES

- Ahumada, J., & Lapasset, E. 1995, *A&AS*, 109, 375
- Bailyn, C. D. 1995, *ARA&A*, 33, 133
- Bellazzini, M., Pasquali, A., Federici, L., Ferraro, F. R., & Pecci, F. F. 1995, *ApJ*, 439, 687
- Benz, W., & Hills, J. G. 1987, *ApJ*, 323, 614
- Bressan, A., Marigo, P., Girardi, L., et al. 2012, *MNRAS*, 427, 127
- Harris, W. E. 1996, *AJ*, 112, 1487
- Caffau, E., Ludwig, H.-G., Steffen, M., Freytag, B., & Bonifacio, P. 2011, *Sol. Phys.*, 268, 255
- Carney, B. W., Latham, D. W., & Laird, J. B. 2005, *AJ*, 129, 466
- Carney, B. W., Gray, D. F., Yong, D., et al. 2008, *AJ*, 135, 892
- Carretta, E., Gratton, R. G., Lucatello, S., Bragaglia, A., & Bonifacio, P. 2005, *A&A*, 433, 597
- Carretta, E., Bragaglia, A., Gratton, R. G., et al. 2009, *A&A*, 505, 117
- Castelli, F., Gratton, R. G., & Kurucz, R. L. 1997, *A&A*, 318, 841
- Castelli, F., & Kurucz, R. L. 2003, *Modelling of Stellar Atmospheres*, 210, 20P
- Clarkson, W. I., Sahu, K. C., Anderson, J., et al. 2011, *ApJ*, 735, 37
- Cortés, C., Silva, J. R. P., Recio-Blanco, A., Catelan, M., Do Nascimento, J. D., & De Medeiros, J. R. 2009, *ApJ*, 704, 750
- De Marco, O., Shara, M. M., Zurek, D., Ouellette, J. A., Lanz, T., Saffer, R. A., & Sepinsky, J. F. 2005, *ApJ*, 632, 894
- Ferraro, F. R., Fusi Pecci, F., & Bellazzini, M. 1995, *A&A*, 294, 80
- Ferraro, F. R., Paltrinieri, B., Fusi Pecci, F., et al. 1997, *A&A*, 324, 915
- Ferraro, F. R., Messineo, M., Fusi Pecci, F., et al. 1999, *AJ*, 118, 1738
- Ferraro, F. R., Possenti, A., Sabbi, E., et al. 2003, *ApJ*, 595, 179

- Ferraro, F. R., Beccari, G., Rood, R. T., et al. 2004, *ApJ*, 603, 127
- Ferraro, F. R., Sabbi, E., Gratton, R., et al. 2006, *ApJ*, 647, L53
- Ferraro, F. R., Beccari, G., Dalessandro, E., et al. 2009, *Nature*, 462, 1028
- Ferraro, F. R., Lanzoni, B., Dalessandro, E., et al. 2012, *Nature*, 492, 393
- Gilliland, R. L., Bono, G., Edmonds, P. D., et al. 1998, *ApJ*, 507, 818
- Gratton, R. G., Carretta, E., Eriksson, K., & Gustafsson, B. 1999, *A&A*, 350, 955
- Grevesse, N., & Sauval, A. J. 1998, *Space Sci. Rev.*, 85, 161
- Hills, J. G., & Day, C. A. 1976, *Astrophys. Lett.*, 17, 87
- Hut, P., McMillan, S., Goodman, J., et al. 1992, *PASP*, 104, 981
- Kaluzny, J., & Thompson, I. B. 2009, *Acta Astron.*, 59, 273
- Kurucz, R. L. 1993, CD-ROM 13, 18 <http://kurucz.harvard.edu>
- Leonard, P. J. T., & Livio, M. 1995, *ApJ*, 447, L121
- Lombardi, J., C., Jr., Rasio, F. A., & Shapiro, S. L. 1995, *ApJ*, 445, L117
- Lovisi, L., Mucciarelli, A., Ferraro, F. R., et al. 2010, *ApJ*, 719, L121
- Lovisi, L., Mucciarelli, A., Lanzoni, B., et al. 2012, *ApJ*, 754, 91, L12
- Lovisi, L., Mucciarelli, A., Lanzoni, B., et al. 2013, *ApJ*, 772, 148
- McCrea, W. H. 1964, *MNRAS*, 128, 335
- Meylan, G., & Heggie, D. C. 1997, *A&A Rev.*, 8, 1
- Michaud, G., Vauclair, G., & Vauclair, S. 1983, *ApJ*, 267, 256
- Momany, Y., Held, E. V., Saviane, I., et al. 2007, *A&A*, 468, 973
- Mucciarelli, A., Salaris, M., Lovisi, L., et al. 2011, *MNRAS*, 412, 81
- Mucciarelli, A., Pancino, E., Lovisi, L., Ferraro, F. R., & Lapenna, E. 2013, *ApJ*, 766, 78
- Mucciarelli, A., Salaris, M., Lanzoni, B., et al. 2013, *ApJ*, 772, L27
- Paresce, F., de Marchi, G., & Ferraro, F. R. 1992, *Nature*, 360, 46

- Pasquini, L., Avila, G., Blecha, A., et al. 2002, *The Messenger*, 110, 1
- Pietrinferni, A., Cassisi, S., Salaris, M., & Castelli, F. 2006, *ApJ*, 642, 797
- Pooley, D., & Hut, P. 2006, *ApJ*, 646, L143
- Preston, G. W., & Sneden, C. 2000, *AJ*, 120, 1014
- Ransom, S. M., Hessels, J. W. T., Stairs, I. H., et al. 2005, *Science*, 307, 892
- Robin, A. C., Reylé, C., Derrière, S., & Picaud, S. 2003, *A&A*, 409, 523
- Sabbi, E., Ferraro, F. R., Sills, A., & Rood, R. T. 2004, *ApJ*, 617, 1296
- Santana, F. A., Muñoz, R. R., Geha, M., et al. 2013, *ApJ*, 774, 106
- Sarna, M. J., & De Greve, J.-P. 1996, *QJRAS*, 37, 11
- Sbordone, L., Bonifacio, P., Castelli, F., & Kurucz, R. L. 2004, *Memorie della Societa Astronomica Italiana Supplementi*, 5, 93
- Shara, M. M., Saffer, R. A., & Livio, M. 1997, *ApJ*, 489, L59
- Sills, A., Adams, T., & Davies, M. B. 2005, *MNRAS*, 358, 716
- Sneden, C., Preston, G. W., & Cowan, J. J. 2003, *ApJ*, 592, 504
- Stetson, P. B., & Pancino, E. 2008, *PASP*, 120, 1332
- Takeda, Y. 1997, *PASJ*, 49, 471
- Tomkin, J., Lemke, M., Lambert, D. L., & Sneden, C. 1992, *AJ*, 104, 1568
- Tonry, J., & Davis, M. 1979, *AJ*, 84, 1511
- Yong, D., Meléndez, J., Grundahl, F., et al. 2013, *MNRAS*, 434, 3542
- Zloczewski, K., Kaluzny, J., Rozyczka, M., Krzeminski, W., & Mazur, B. 2012, *Acta Astron.*, 62, 357

ID	RA (degrees)	DEC (degrees)	V	I	$T_{eff}$ (K)	$\log(g)$	RV ( $\text{km s}^{-1}$ )	$v_e \sin(i)$ ( $\text{km s}^{-1}$ )	[Fe II/H]	[O/H]	[C/H]	Notes
BSS1	287.7410103	-59.9633904	15.49	15.27	8241	4.0	$-22.6 \pm 0.1$	$11 \pm 1$	$-1.22 \pm 0.09$	$-1.71 \pm 0.17$	$-1.69 \pm 0.14$	PM
BSS2	287.7168646	-59.9846242	15.62	15.48	9204	4.3	$-24.7 \pm 0.8$	$35 \pm 1$	$-0.96 \pm 0.05$	$-2.31 \pm 0.03$	$-2.30 \pm 0.06$	
BSS3	287.7039030	-59.9910308	16.45	15.88	6808	4.0	$-19.5 \pm 1.5$	$11 \pm 2$	$-1.59 \pm 0.09$	$-1.65 \pm 0.11$	$-1.45 \pm 0.07$	
BSS4	287.6827377	-59.9749054	16.59	16.15	7447	4.2	$-23.7 \pm 2.2$	$20 \pm 2$	$-1.54 \pm 0.08$	$-1.35 \pm 0.08$	$-1.65 \pm 0.10$	
BSS5	287.6897573	-59.9918788	16.71	16.11	6730	4.0	$-29.5 \pm 1.1$	$0 \pm 1$	$-1.67 \pm 0.17$	$-1.48 \pm 0.15$	$-1.27 \pm 0.08$	PM
BSS6	287.6872156	-60.0099633	16.70	16.23	7161	4.1	$-27.2 \pm 0.7$	$19 \pm 2$	$-1.57 \pm 0.12$	–	–	$\gamma$ Dor
BSS7	287.7208140	-59.9780412	16.74	16.13	6730	4.0	$-22.7 \pm 0.9$	$16 \pm 5$	$-1.58 \pm 0.12$	$-1.47 \pm 0.14$	$-1.43 \pm 0.07$	
BSS8	287.7141443	-59.9718582	16.72	16.38	7727	4.4	$-23.6 \pm 1.3$	$25 \pm 5$	$-1.32 \pm 0.13$	$-1.19 \pm 0.08$	$-1.75 \pm 0.06$	
BSS9	287.6997850	-59.9785210	17.11	16.63	7244	4.3	$-33.3 \pm 0.2$	$13 \pm 7$	$-1.58 \pm 0.10$	$-1.82 \pm 0.07$	$-1.99 \pm 0.06$	
BSS10	287.7669498	-59.9853719	15.33	15.19	9016	4.1	$-24.6 \pm 0.7$	$0 \pm 1$	$-0.46 \pm 0.08$	$-2.68 \pm 0.06$	$-2.06 \pm 0.06$	PM, EHB
BSS11	287.7252708	-60.0033895	15.74	15.26	7482	3.9	$-17.3 \pm 4.4$	$38 \pm 1$	$-1.35 \pm 0.14$	$-1.34 \pm 0.08$	$-1.62 \pm 0.10$	PM, SX-Phe
BSS12	287.7294365	-59.9826813	16.24	15.91	7889	4.2	$-27.1 \pm 1.3$	$24 \pm 4$	$-1.48 \pm 0.11$	$-1.87 \pm 0.06$	$-2.03 \pm 0.04$	
BSS13	287.7299968	-59.9810128	16.65	16.06	6714	4.0	$-14.1 \pm 1.7$	$28 \pm 2$	$-1.43 \pm 0.14$	–	–	
BSS14	287.7546346	-59.9891338	16.63	16.19	7379	4.2	$-35.0 \pm 0.4$	$0 \pm 2$	$-1.54 \pm 0.10$	$-1.28 \pm 0.08$	$-1.41 \pm 0.10$	PM
ID	RA (degrees)	DEC (degrees)	B	R	$T_{eff}$ (K)	$\log(g)$	RV ( $\text{km s}^{-1}$ )	$v_e \sin(i)$ ( $\text{km s}^{-1}$ )	[Fe II/H]	[O/H]	[C/H]	Notes
BSS15	287.7851741	-60.0189240	16.17	15.68	7194	3.9	$-23.4 \pm 0.4$	$0 \pm 1$	$-1.57 \pm 0.08$	$-1.23 \pm 0.17$	$-1.70 \pm 0.17$	PM
BSS16	287.7918025	-59.9806129	16.83	16.31	6934	4.1	$-35.5 \pm 0.1$	$17 \pm 4$	$-1.58 \pm 0.16$	$-1.40 \pm 0.09$	$-1.86 \pm 0.06$	PM
BSS17	287.6424824	-59.9491533	16.21	15.83	7413	4.0	$-23.4 \pm 3.6$	$28 \pm 2$	$-1.45 \pm 0.07$	$-1.09 \pm 0.13$	$-1.81 \pm 0.08$	PM, SX-Phe
BSS18	287.5595535	-60.0844359	16.35	16.04	7870	4.2	$-32.8 \pm 0.1$	$29 \pm 5$	$-1.52 \pm 0.17$	$-1.01 \pm 0.20$	$-1.33 \pm 0.08$	

Table 1: Identification numbers, coordinates, magnitudes, effective temperatures, surface gravities, radial and rotational velocities, Fe, O and C abundances of the BSSs in the ACS (on the top) and WFI (on the bottom) samples. PM indicates BSSs with proper motion by Zloczewski et al. (2012);  $\gamma$ Dor, EHB and SX-Phe are  $\gamma$ Dor pulsator stars, Extreme Horizontal Branch stars and SX-Phoenixis stars according to Kaluzny & Thompson (2009).

ID	RA (degrees)	DEC (degrees)	B	R	$T_{eff}$ (K)	$\log(g)$	RV (km s <sup>-1</sup> )	$v_e \sin(i)$ (km s <sup>-1</sup> )	[Fe I/H]
RGB1	287.8801804	-60.0657549	15.71	14.75	5321	2.9	-31.0 ± 0.4	0 ± 1	-1.49 ± 0.19
RGB2	287.8762748	-60.0447351	16.34	15.41	5420	3.2	-23.9 ± 0.4	0 ± 1	-1.58 ± 0.18
RGB3	287.8683233	-60.0417224	16.17	15.22	5395	3.2	-30.0 ± 0.4	0 ± 1	-1.66 ± 0.17
RGB4	287.8715668	-60.0333950	16.16	15.22	5395	3.2	-23.9 ± 0.3	0 ± 1	-1.55 ± 0.18
RGB5	287.9149051	-59.9760061	16.35	15.41	5420	3.2	-26.4 ± 0.4	3 ± 4	-1.61 ± 0.21
RGB6	287.9489041	-59.9747585	16.07	15.13	5383	3.1	-23.9 ± 0.4	0 ± 1	-1.60 ± 0.18
RGB7	287.9380203	-60.0425142	16.03	15.09	5383	3.1	-20.1 ± 0.3	0 ± 1	-1.52 ± 0.21
RGB8	287.6115858	-60.1160018	16.38	15.44	5433	3.3	-29.0 ± 0.3	0 ± 1	-1.52 ± 0.24
RGB9	287.7844635	-60.0714674	16.40	15.47	5433	3.3	-22.7 ± 0.3	0 ± 1	-1.49 ± 0.21
RGB10	287.5961780	-60.0743004	16.23	15.28	5395	3.2	-26.3 ± 0.3	0 ± 1	-1.46 ± 0.22
RGB11	287.7903486	-60.0508958	15.77	14.79	5333	3.0	-32.3 ± 0.4	0 ± 1	-1.60 ± 0.22
RGB12	287.7629329	-60.0411150	16.20	15.27	5395	3.2	-28.9 ± 0.4	0 ± 1	-1.62 ± 0.20
RGB13	287.7711636	-60.0293473	16.35	15.42	5433	3.3	-18.3 ± 0.5	6 ± 6	-1.58 ± 0.17
RGB14	287.8302739	-60.0643595	15.87	14.92	5358	3.1	-26.8 ± 0.3	0 ± 1	-1.55 ± 0.21
RGB15	287.7805513	-60.0460663	16.35	15.41	5420	3.2	-33.4 ± 0.4	0 ± 1	-1.53 ± 0.22
RGB16	287.8110505	-60.0122533	16.47	15.54	5458	3.3	-36.5 ± 0.4	5 ± 4	-1.61 ± 0.20
RGB17	287.5672807	-60.0886491	16.42	15.51	5433	3.3	-24.9 ± 0.3	0 ± 1	-1.49 ± 0.20
RGB18	287.4885332	-60.0152793	16.25	15.31	5420	3.2	-26.4 ± 0.4	0 ± 1	-1.46 ± 0.19
RGB19	287.4794481	-60.0369896	16.42	15.47	5433	3.3	-24.2 ± 0.5	0 ± 1	-1.51 ± 0.22
RGB20	287.4514453	-60.2169573	15.86	14.88	5333	3.0	-23.5 ± 0.3	0 ± 1	-1.40 ± 0.22
RGB21	287.5688340	-60.1870682	16.32	15.38	5420	3.2	-27.9 ± 0.3	0 ± 1	-1.35 ± 0.23
RGB22	287.6634437	-60.1823294	16.29	15.36	5420	3.2	-24.7 ± 0.4	0 ± 1	-1.49 ± 0.21
RGB23	287.6113178	-60.1784682	16.39	15.48	5433	3.3	-30.0 ± 0.4	0 ± 1	-1.53 ± 0.23
RGB24	287.7655149	-60.1501678	15.82	14.86	5333	3.0	-27.8 ± 0.3	0 ± 1	-1.49 ± 0.19
RGB25	287.7063369	-60.1300567	16.42	15.54	5458	3.3	-23.3 ± 0.3	0 ± 1	-1.57 ± 0.26
RGB26	287.8546812	-60.1840216	16.13	15.19	5395	3.2	-29.5 ± 0.3	0 ± 1	-1.51 ± 0.24

Table 2: Identification numbers, coordinates, magnitudes, effective temperatures, surface gravities, radial and rotational velocities and Fe abundance of the RGB sample.

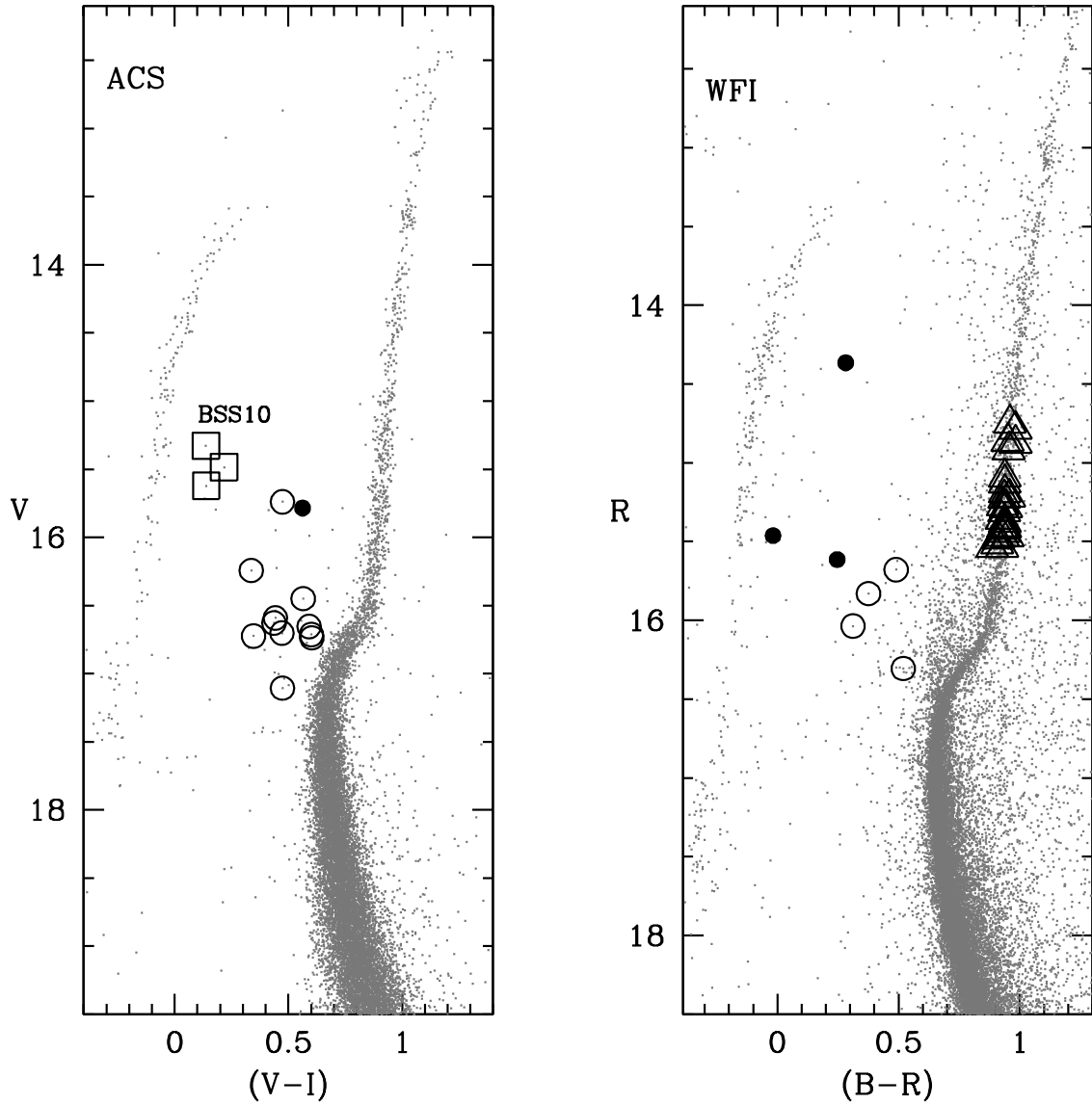


Fig. 1.— Colour-magnitude diagrams of NGC 6752 for the ACS and WFI datasets. Open circles, squares and large black dots are the observed BSSs; open triangles are the observed RGB stars. Large black dots are BSSs turned out to be field stars whereas open squares are BSSs affected by radiative levitation.

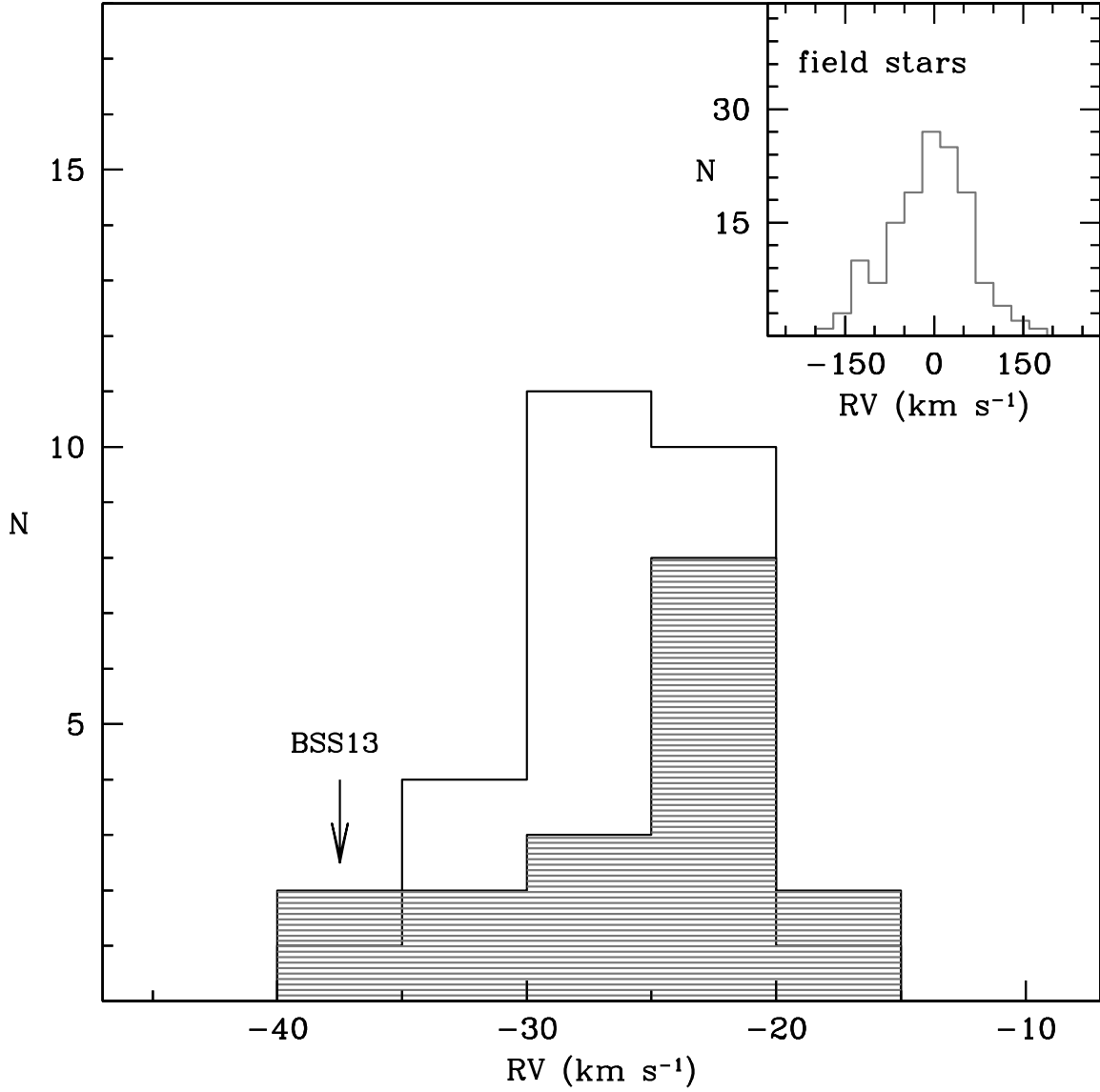


Fig. 2.— Radial velocity distributions for the RGB stars (empty histogram) and the likely member BSSs (grey shaded histogram). The inset shows the radial velocity distribution of field stars according to models by Robin et al. (2003).

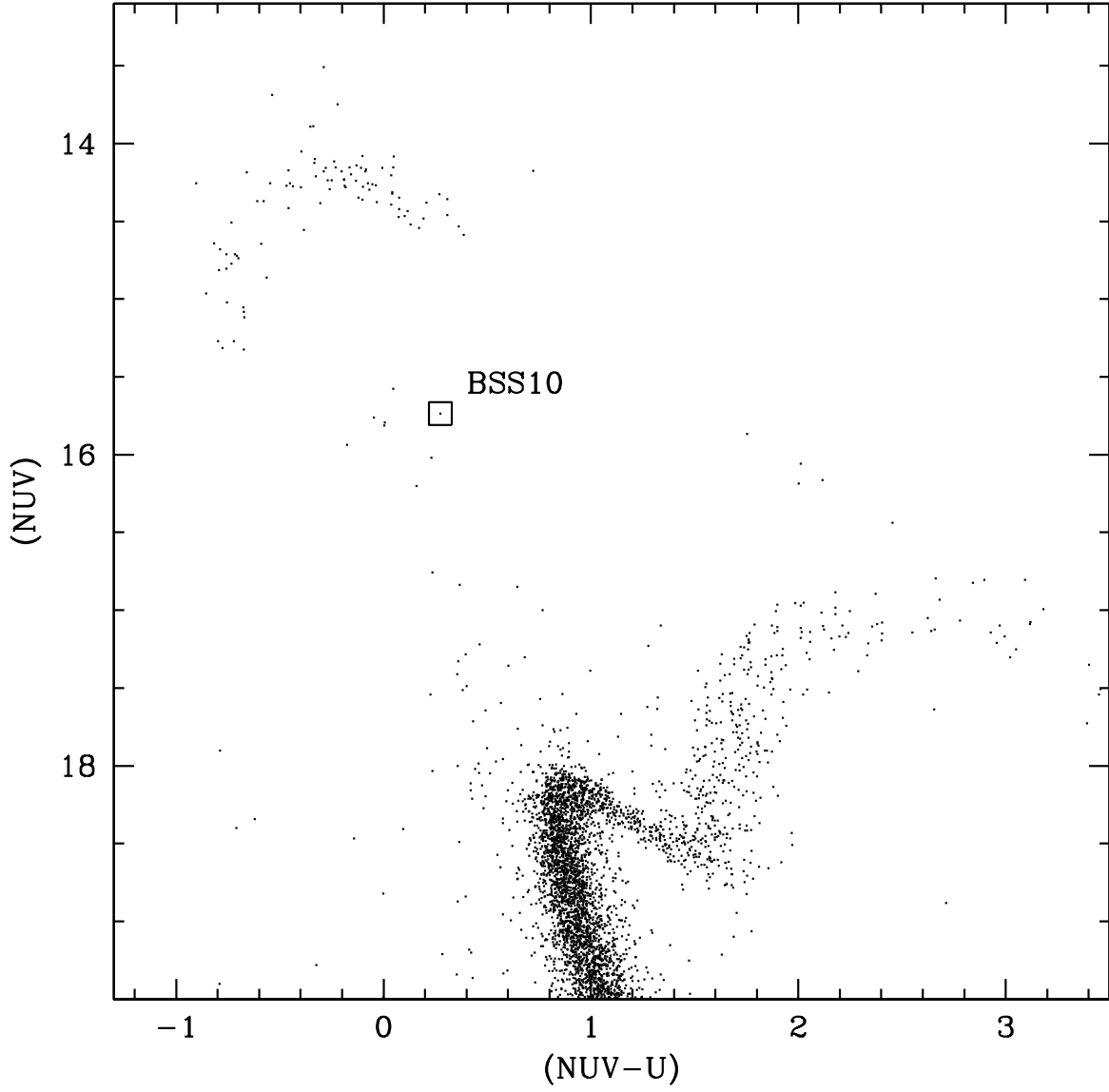


Fig. 3.— CMD in the UV plane obtained from WFPC2 observations of NGC 6752 (Sabbi et al. 2004). The open square marks the position of BSS10.

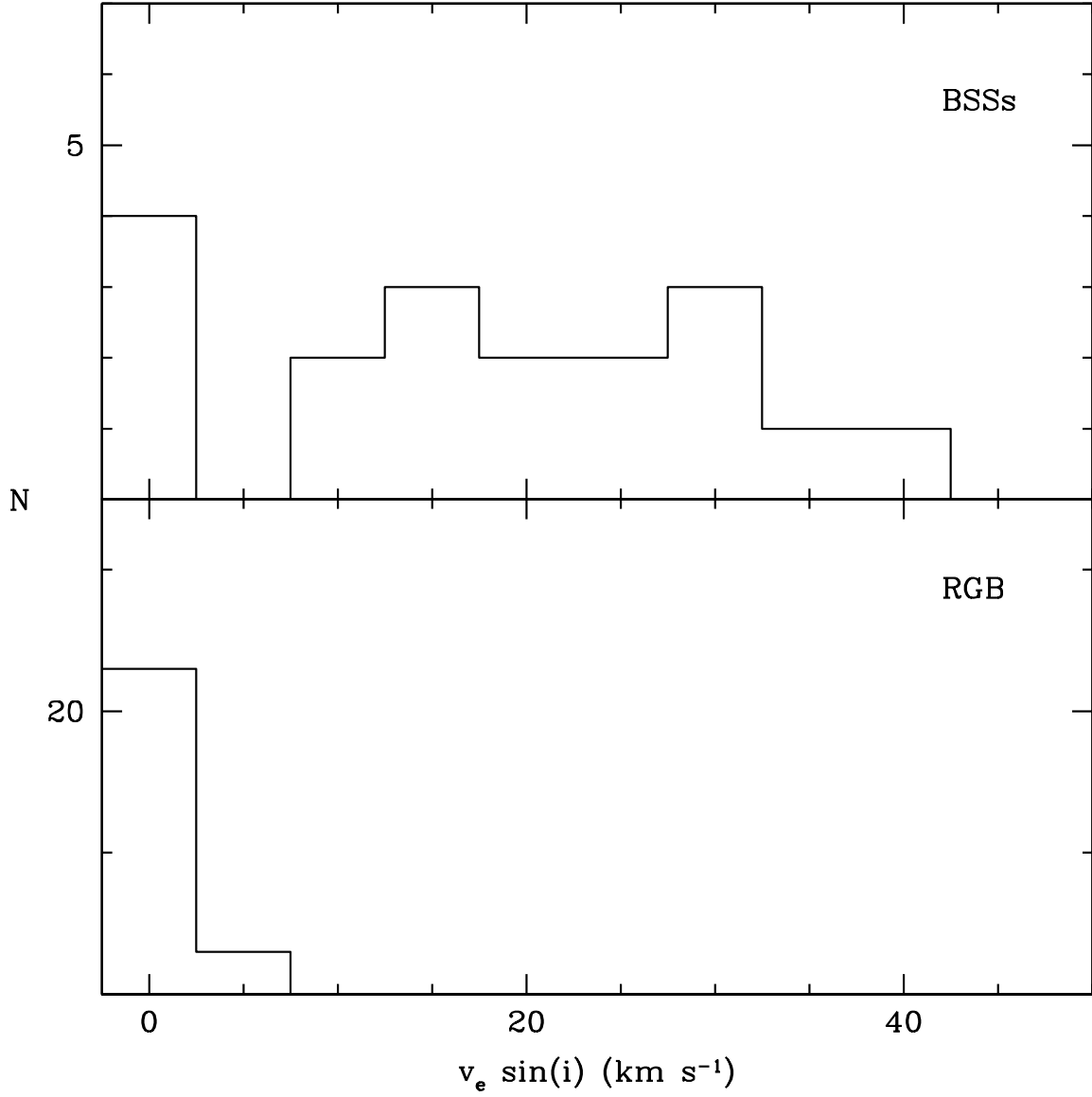


Fig. 4.— Rotational velocity distributions for BSSs (upper panel) and RGB stars (lower panel).

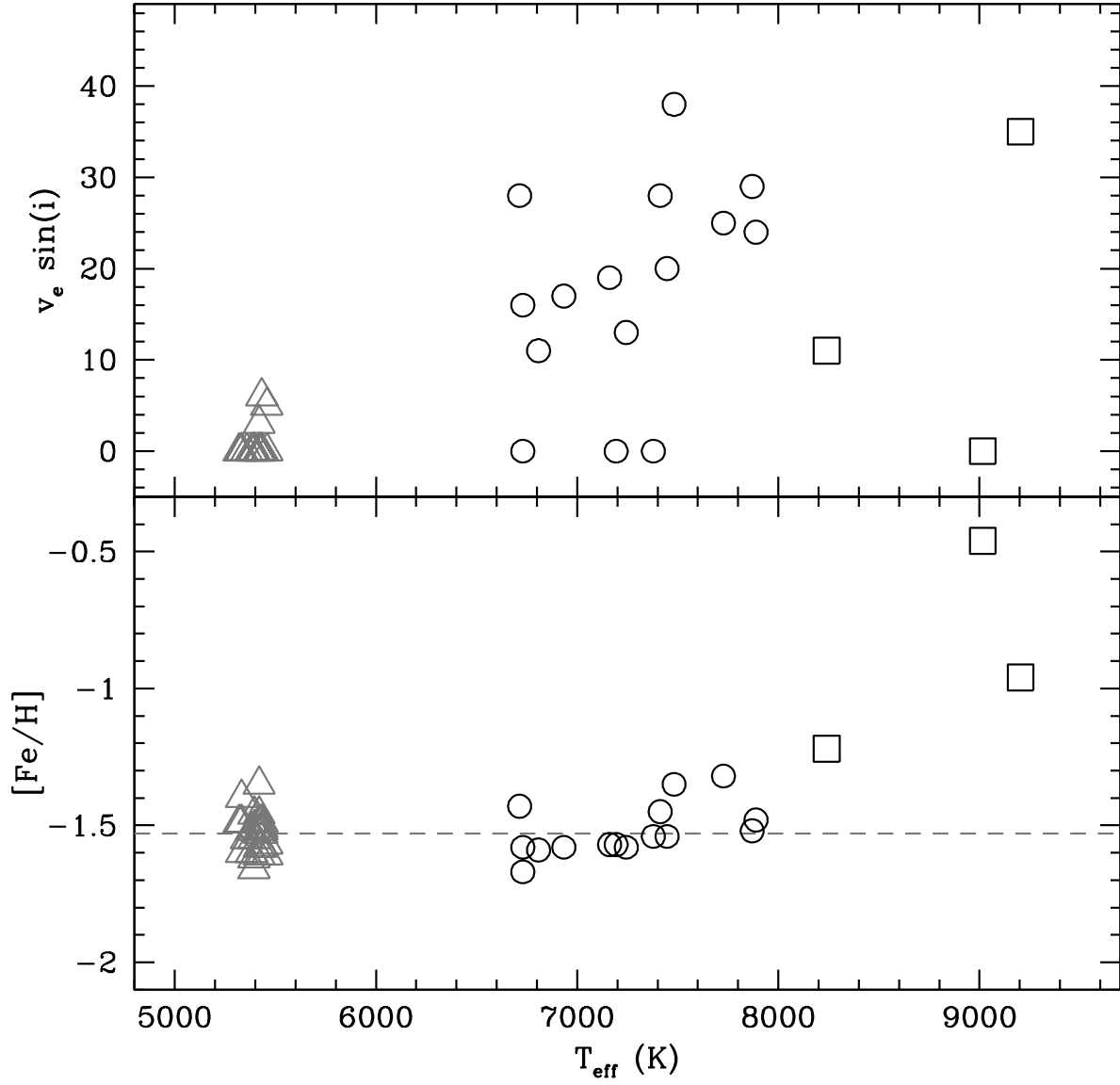


Fig. 5.— Upper panel: rotational velocities for RGB stars (grey triangles) and BSSs (circles and squares) as a function of temperatures. Lower panel: iron abundances for RGB stars and BSSs. The dashed horizontal line defines the mean Fe abundance of RGB stars. Squares are BSSs affected by radiative levitation.

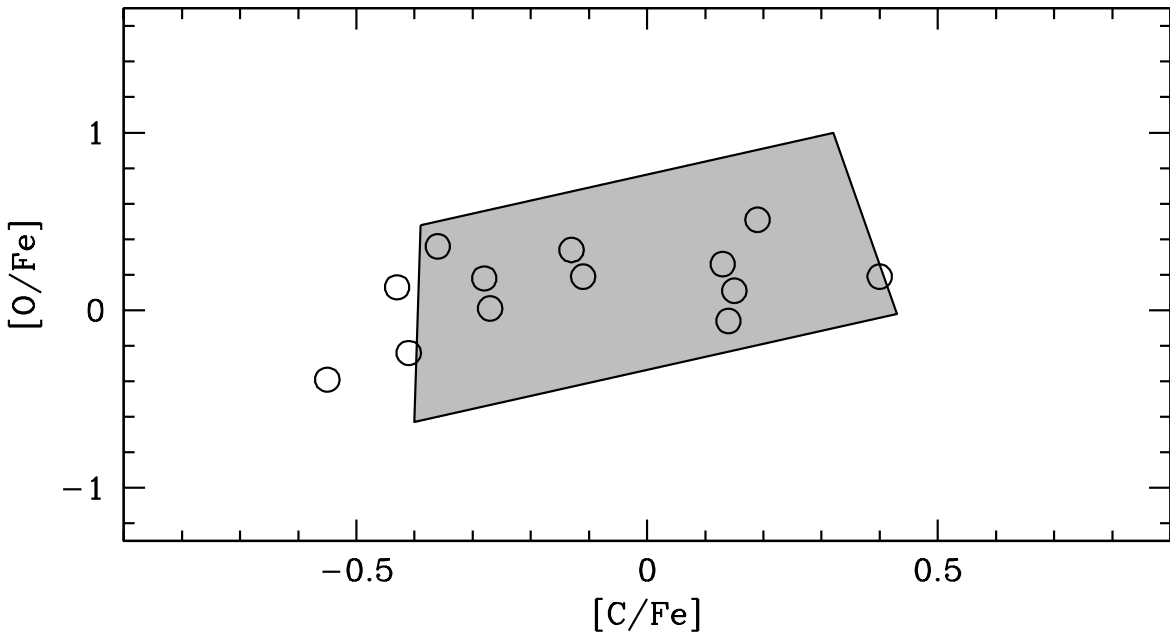


Fig. 6.—  $[C/Fe]$  and  $[O/Fe]$  ratios of BSSs (open circles) compared with those of dwarf stars (grey region).

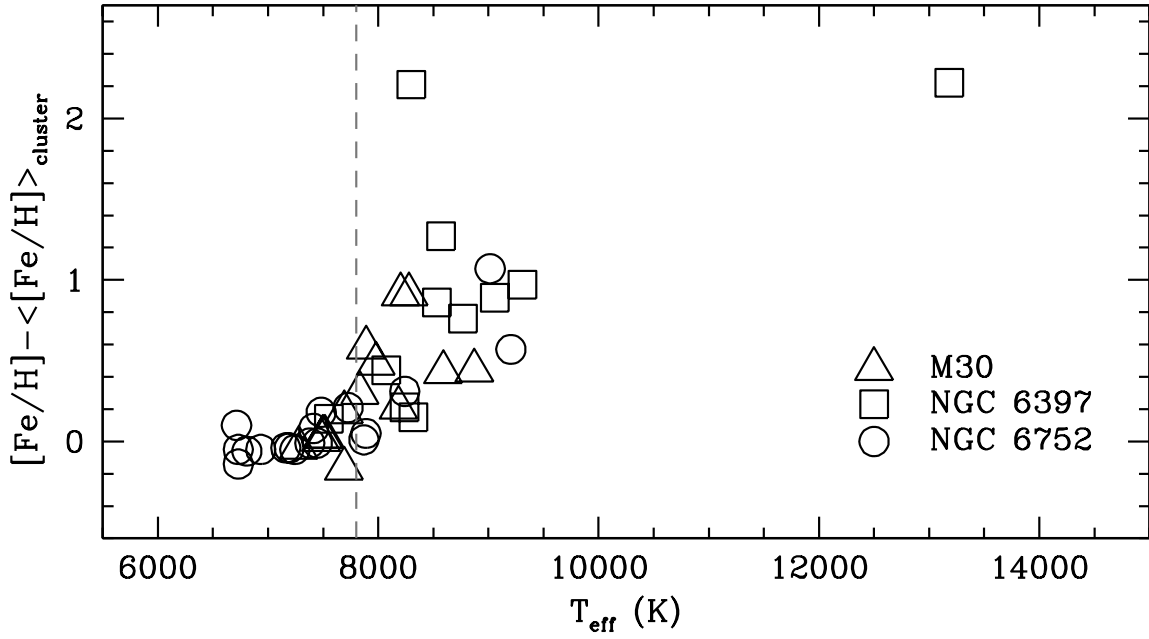


Fig. 7.—  $[\text{Fe}/\text{H}]$  ratios (scaled to the mean metallicity of the clusters) as a function of temperature for BSSs in M30 (triangles, Lovisi et al. 2013), NGC 6397 (squares, Lovisi et al. 2012) and NGC 6752 (circles, this work). The dashed vertical line marks the temperature threshold for the onset of radiative levitation ( $T_{\text{eff}}=7800\text{K}$ ).